UNCLASSIFIED

INITIAL RESULTS OF THE ARMY BACKGROUND EXPERIMENT (U)

W. C. Feldman, G. F. Auchampaugh, and E. R. Shunk

University of California, Los Alamos National Laboratory,
MS D438, Los Alamos, NM 87545

ABSTRACT. (U) The Army Background Experiment was commissioned in April 1987 to measure the space neutron background near the Earth. It was launched aboard the LACE spacecraft in February 1990 and has operated flawlessly since turn on. An overview of the experiment and initial results from space are presented. Preliminary analysis indicates that all experimental objectives should be achieved within the nominal 30-month lifetime of LACE.

INTRODUCTION (U)

(U) The Army Background Experiment was commissioned by the U.S. Army Strategic Defense Command as part of its mass-sensor development program. Its goals were to 1) measure the energy spectrum of atmospheric leakage neutrons in the range between 0.5 MeV and 20 MeV, 2) develop a leakage-neutron data base as a function of geomagnetic latitude and solar activity, 3) develop a predictive capability by correlating the resultant ABE data base with the extensive solar-terrestrial data base archived by NOAA and the NSSDC, 4) estimate the angular anisotropy of terrestrial leakage neutrons by measuring their horizon-to-zenith-directed flux ratio, and 5) estimate the spacecraft-generated neutron-flux spectrum.

(U) Major milestones for ABE began with 1) conception in April 1987, 2) a first fit-check delivery to NRL in April 1988, 3) calibration at Los Alamos in October 1988, 4) final delivery to NRL for LACE integration and environmental tests in October 1988, 5) launch from Kennedy Space Center on 14 February 1990, and 6) experiment power up on 26 February 1990. Analyses of first-look data measured on orbit through 30 April 1990, show that ABE is working flawlessly and promises to fulfill all programmatic requirements of its mission. The rest of this paper will present an overview of the experiment and a survey of initial results.

THE ABE SENSOR (U)

(U) The ABE sensor consists of four, close packed, 3-inch diameter by 8-inch long rods of borated plastic scintillator as shown in Figure 1. It is mounted on the underside of one of four fold-out panels of the LACE spacecraft. The arrangement of the rods is such that one of the rods (designated as rod number two) has a clear fan-shaped field of view of atmospheric leakage neutrons that is offset from the nadir (toward earth) by 45°, and one of the rods (designated as rod number 3) has a clear, fan-shaped field of view of spacecraft-generated neutrons that is offset from the zenith by 45°.

(U) The principle of operation of the ABE sensor is illustrated in the right half of Figure 1. It acts like an electronically black (or totally absorbing) detector by selecting for analysis, only those neutrons that lose all their sensible energy to proton recoil, elastic scattering interactions in the scintillators. This type of event is signaled by the occurrence of a characteristic, time-correlated double event. Whereas the first of an event pair corresponds to energy deposition in the scintillator resulting from multiple proton-recoil interactions, the second of an event pair corresponds to occurrence of the $^{10}B(n, \alpha)\,^{7}Li$ reaction.

Accession Number: 4900

Title: Initial Results of the Army Background Experiment

Personal Author: Feldman, W.C.; Auchampaugh, G.F.; Shunk, E.R.

Corporate Author Or Publisher: Los Alamos National Laboratory, Los Alamos, NM 87545

Descriptors, Keywords: Army Background Experiment Space Neutron LACE USASDC Sensor ABE Environment Radiation

Pages: 00011

Cataloged Date: Feb 17, 1994

Document Type: HC

Number of Copies In Library: 000001

Record ID: 28653

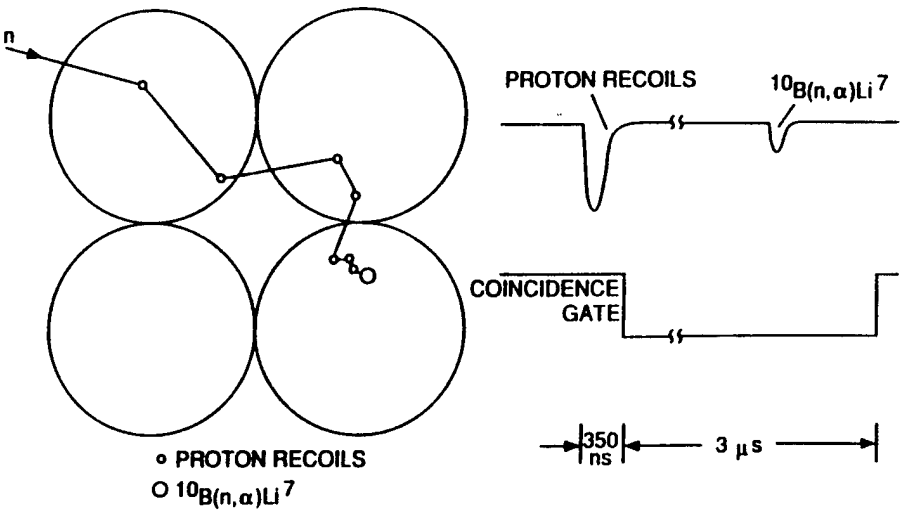

Figure 1. Schematic drawing of the ABE sensor illustrating its principle of operation.

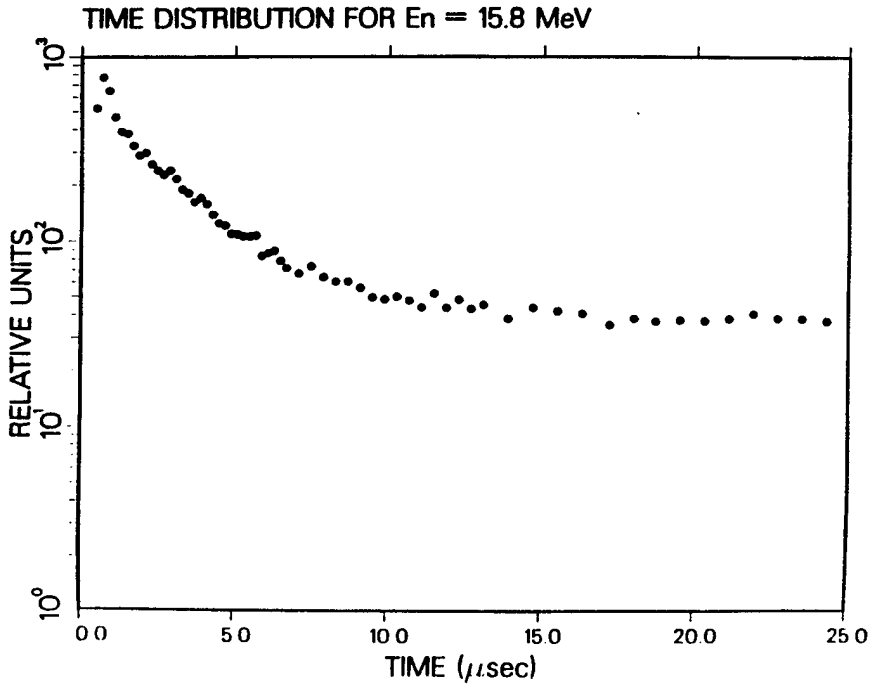

Figure 2. The spectrum of time differences between first and second interactions of event pairs for monoenergetic 15.8 MeV neutrons.

Pre-Launch Tests (U)

(U) Proper operation of ABE was verified by calibration at Los Alamos using Van de Graaff-generated monoenergetic neutron beams ranging in energy from 0.6 MeV to 20 MeV and an ^{241}Am-^{11}B isotopic neutron source that emits a flux spectrum peaked at about 3.1 MeV. Verification at NRL aboard LACE was made using a ^{252}Cf isotopic neutron source. An example of the distribution of elapsed times between first and second pulses for monoenergetic 15.8 MeV neutrons is shown in Figure 2. The upturn at early times corresponds to the correlation resulting from stopping the incident neutron in the scintillator while the flat portion of the curve at late times corresponds to chance coincidences. When the chance coincidences are subtracted from the total spectrum, a single, exponentially-decaying spectrum remains. A fit to the subtracted spectrum, shown by the solid line in Figure 3, yields a time constant, $\tau = 2.4$ μs. This value is close to that expected, $\tau = (N_{10_B}\sigma v)^{-1} = 2.2$ μs, for a plastic scintillator containing 5 weight percent of natural boron.

(U) A study of the causes of the discrepancy between the measured time constant of 2.4 μs and the calculated time constant of 2.2 μs was made using other measurements having better statistics. This study revealed that the relation between the coincidence count rate and the time elapsed from detection of a first interaction is slightly concave upwards. A fit to data in the time interval spanning 0.5 μs to 4.5 μs yields a time constant of about $\tau = 2.2$ μs. A fit to the interval spanning 1.6 μs to 6.0 μs yields $\tau = 2.4$ μs. Note, the solid line in Figure 3 was drawn to fit measured rates between 1.4 μs and 14.3 μs. We speculate that the cause of this effect comes from moderated but escaping neutrons that subsequently return to the sensor after reflecting from nearby material such as the sensor housing or its physical support hardware.

(U) The pulse-height spectrum of second interactions following moderation of the 15.8 MeV neutrons is shown in Figure 4. The peak near 0.1 MeV equivalent electron energy corresponds to the alpha particle and ^{7}Li recoils without detection of the 478 keV gamma ray coming from deexcitation of the first excited state of ^{7}Li. This effective energy is much less than the total energy of the recoiling ions, ~2.3 MeV, because of the nonlinear response of plastic scintillator to heavy ions. The broad peak to the right of the main peak comes from detection of the Compton electron associated with the 478 keV gamma ray.

(U) An example of the spectrum of first interactions, contingent on detection of a second interaction, for 1 MeV monoenergetic neutrons is shown in Figure 5. This spectrum was registered by one of the two rods facing the beam and subject to the additional condition that one, and only one rod detected a first pulse having equivalent electron energy above 35 keV. The spectrum as recorded was then corrected for chance coincidences and transformed to energy in accordance with the measured neutron energy to equivalent electron energy calibration curve.

POST-LAUNCH OPERATION (U)

(U) Launch of ABE aboard the LACE spacecraft into low-Earth orbit did not change its operational state significantly. Several orbits soon after power up were devoted to photomultiplier gain calibration to check for changes resulting from the launch vibration environment. The $^{10}B(n,\alpha)^{7}$ Li peak was used for this purpose. Resulting spectra showed that any such gain changes were less than $\pm 10\%$.

(U) Data can be recorded according to several formats that are set by ground command. Two such formats have been used most frequently; normal mode and single-rod first-interaction mode. In both modes, the first quarter of instrument memory stores pulse height spectra of all sensor events regardless of detection of a second interaction within 26 μs of detection of a first interaction. The spectra provide an overview of the radiation environment experienced by LACE. They clearly show passage through the south Atlantic anomaly and both the north and south horns of the

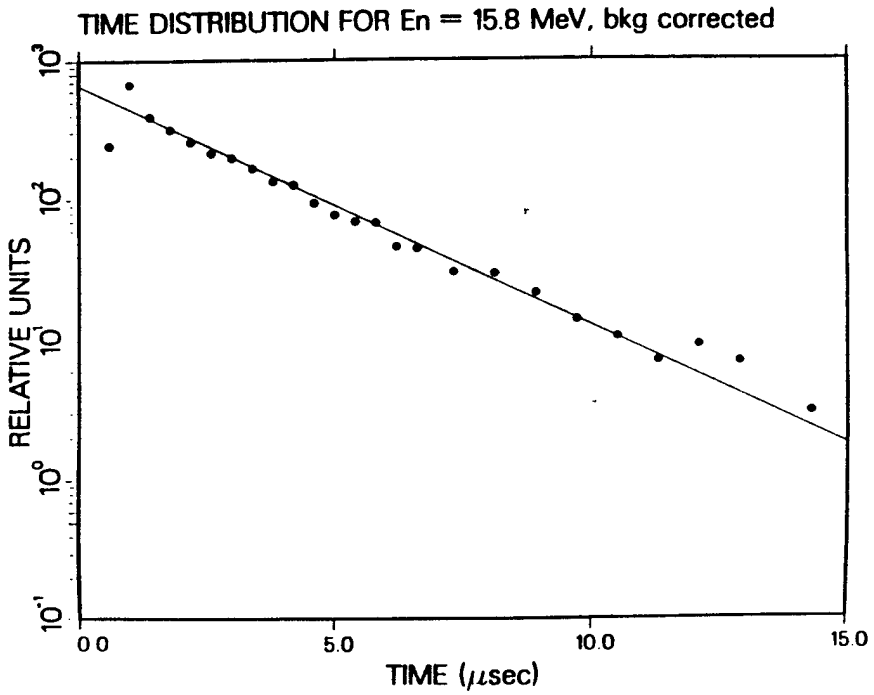

Figure 3. (U) A linear-least-squares fit of a decaying exponential to the time spectrum shown in Figure 2 after a constant rate, due to chance coincidences, is subtracted off.

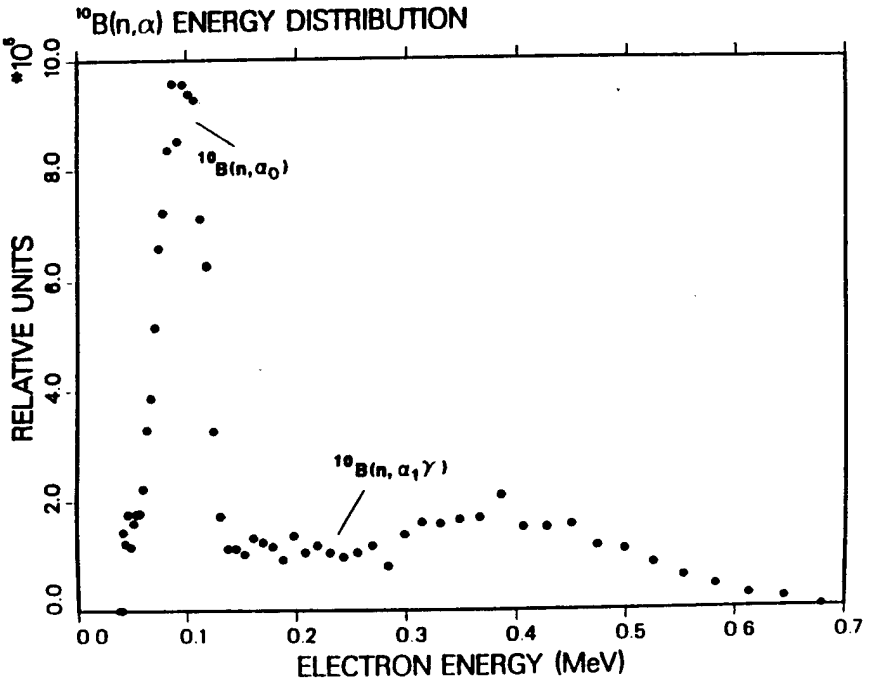

Figure 4. (U) The pulse-height spectrum of second interactions of event pairs resulting from irradiation of the ABE sensor by monoenergetic 15.8 MeV neutrons.

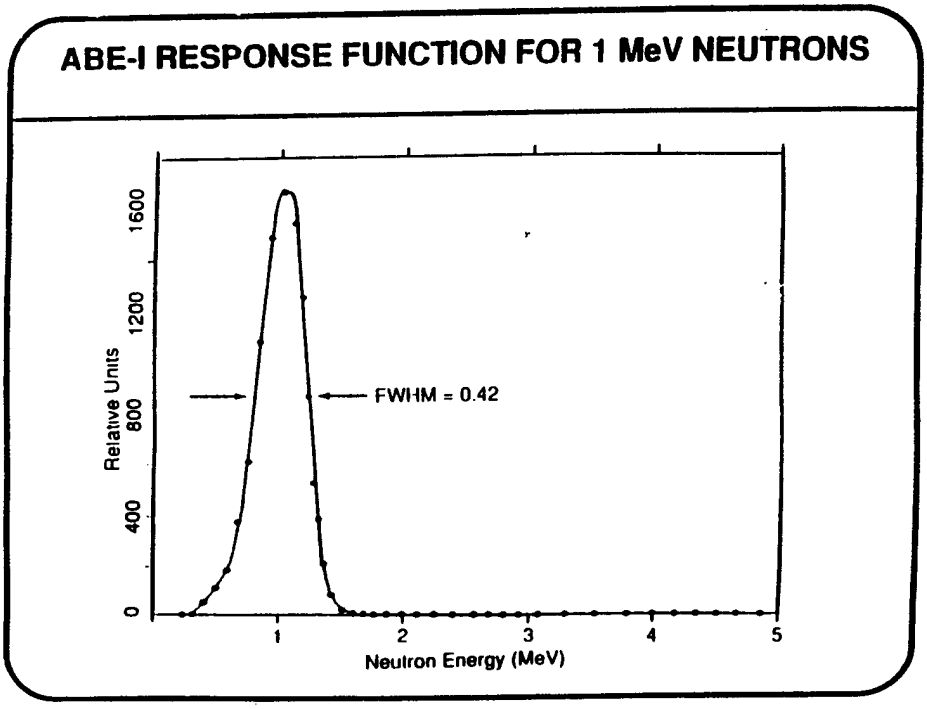

Figure 5. (U) The response function of the ABE sensor to monoenergetic 1 MeV neutrons generated using a Van de Graaff accelerator.

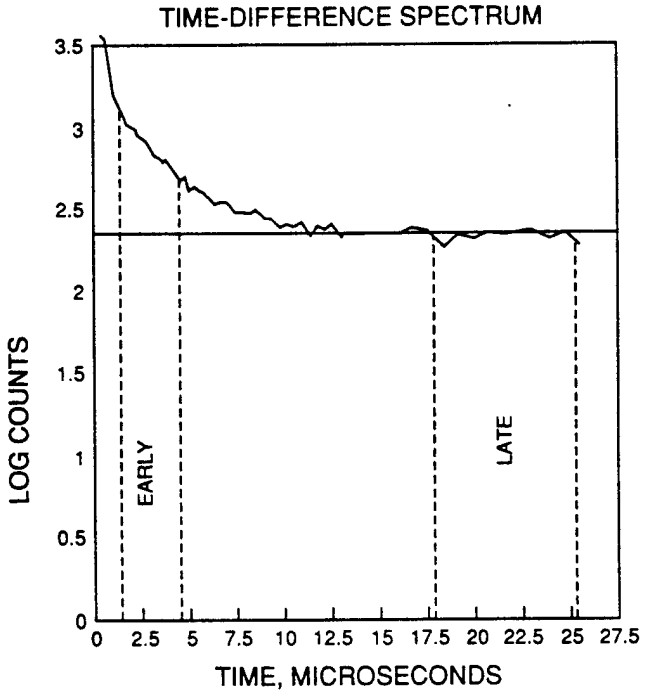

Figure 6. (U) The spectrum of time differences between first and second interactions of event pairs recorded by ABE in orbit on 8 March 1990.

magnetosphere, by significantly enhanced event rates. In between are regions of moderate event rates (less than 5000 s^{-1}). These regions will be used to determine the spectrum of terrestrial leakage neutrons. We focus on a preliminary characterization of these data in the rest of this paper.

(U) The signature of a neutron that has lost all its sensible energy in the ABE sensor is a time-correlated double-pulse event. However, detection of a double-pulse event does not necessarily signify a neutron. Such events can also result from chance coincidences of uncorrelated events, phototube afterpulsing, and the stoppage and subsequent decay of muons. All three of these event types are present in the data and can be accounted for through the application of appropriate filters. They will be illustrated next for the half of orbit 345 that brackets the geomagnetic equator starting at 6:09 UT on 8 March, 1990 near Blossom Point, Maryland.

i) Chance Coincidences (U)

(U) The time rate of second interactions detected after first interactions that deposit sensible energy in one and only one rod of ABE is shown in Figure 6. Three segments of the curve are distinguishable. At late times the detected rate becomes independent of time as indicated by the horizontal line in the figure. Such behavior is expected for chance coincidences. When this "background" is subtracted off, the time dependence of residual second interaction rates is as shown in Figure 7.

ii) Neutron Initiated Events (U)

(U) The two segments of the data in Figure 7 are delineated by the two linear-least-squares fits to exponentials, drawn as straight lines in the log-linear plot. Using a fit interval spanning 1.0 to 4.7 μs, yields a time constant of 2.4 μs. The close equality of this time dependence with that measured during ground calibration as illustrated in Figure 3, allows a tentative identification in terms of neutrons that moderate in the ABE scintillators followed by capture in the $^{10}B(n,\alpha)^7$Li reaction. This identification is further supported by the measured pulse height distribution of second interactions shown in Figure 8. This spectrum was generated by separately selecting all events having first-to-second pulse times within the early and late time intervals shown in Figure 6. The spectrum of second interactions in Figure 8 is then the difference between early and late time gates weighted according to the relative time widths of each gate. Comparison with the spectrum of second events shown in Figure 4 leaves little doubt that our identification in terms of incident fast neutrons is correct.

iii) After Pulsing (U)

(U) Identification of the origin of the early-time upturn in Figure 7 is straightforward. Energy spectra of first- and second-pulse interactions gated on second interaction relative times less than 0.7 μs are shown in the upper two panels of Figure 9. Concentrating first on the energy spectrum of first interactions in the upper left hand panel, we note a predominance of high energy depositions. This effect was measured during flight qualification tests made on each of the photomultiplier tubes before they were integrated into the sensor. We also note that the energy spectrum of second interactions for this time gate shown in the upper right hand panel is very different from that resulting from $^{10}B(n,\alpha)^7$Li shown in Figure 8.

(U) This identification is supported further by the spectra shown in the lower two panels of Figure 9. Here, the second-to-first interaction time distribution (bottom left) and second interaction pulse height distribution (bottom right) gated on greater than 20 MeV equivalent electron energy first interactions are presented. We note that very low time differences dominate the time spectrum

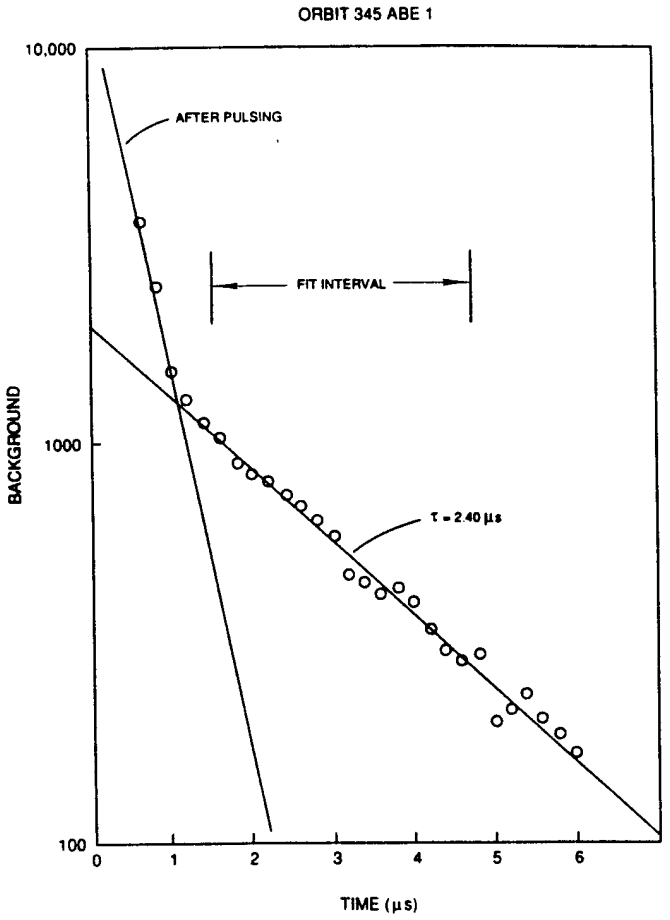

Figure 7. (U) Linear-least-squares fit of a decaying exponential to the time spectrum shown in Figure 6 after a constant rate due to chance coincidences is subtracted off.

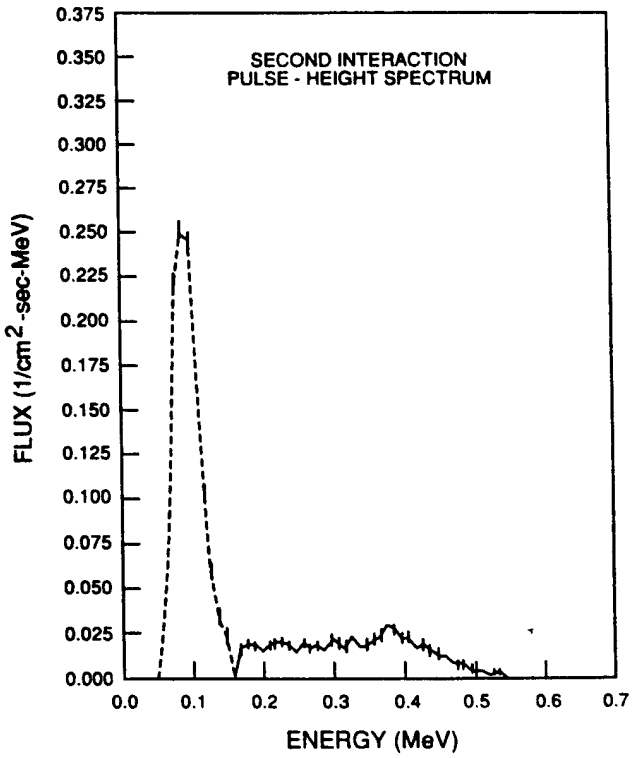

Figure 8. (U) The pulse height spectrum of second interactions of event pairs for ABE in orbit on 8 March 1990. The measured data were filtered to include only time intervals between 1.4 and 4.7 μs, with chance coincidences subtracted off.

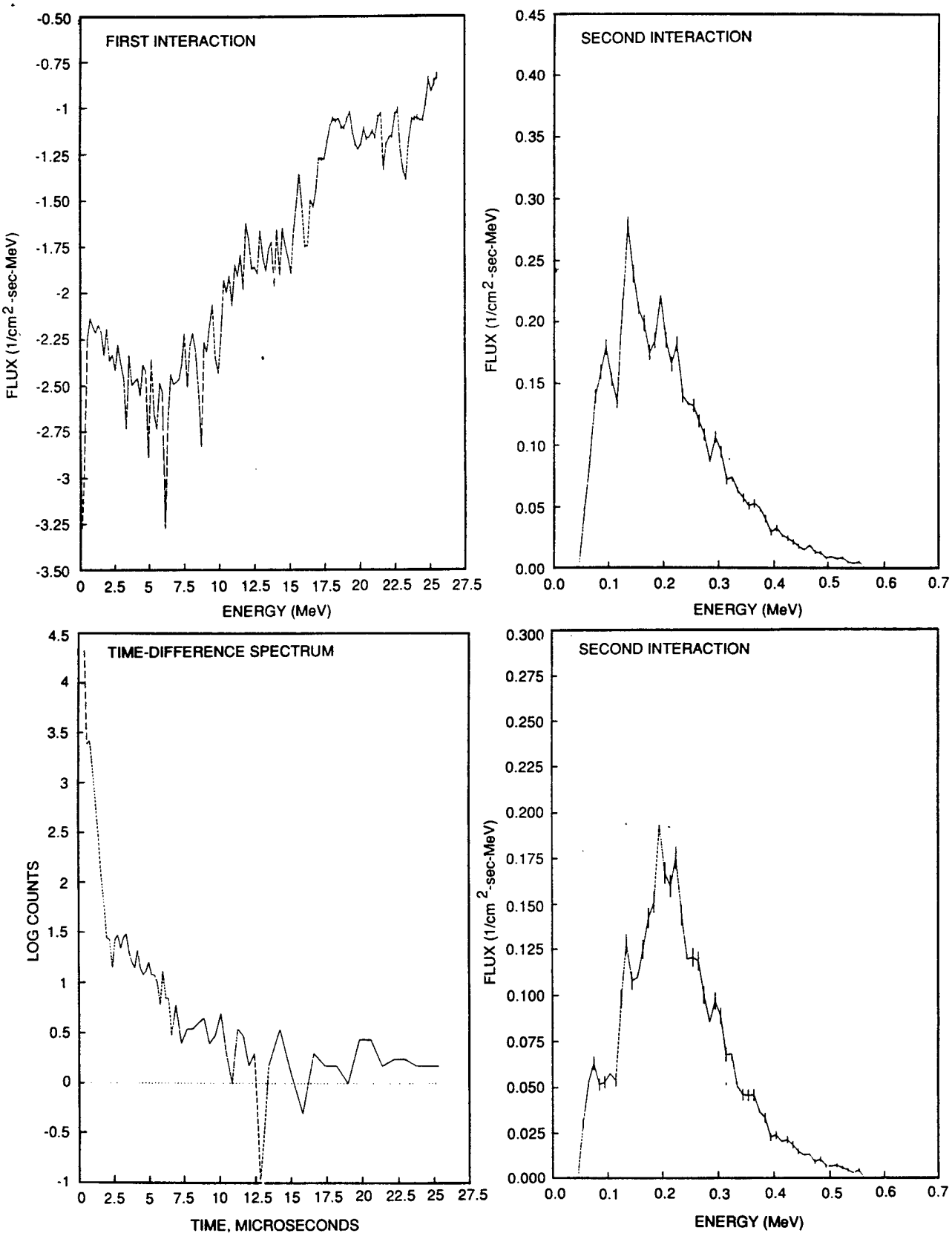

Figure 9. Filters applied to ABE event-mode data in orbit that indicate that the early time upturn in the time spectrum shown in Figures 6 and 7 is due to after pulsing. The upper two panels show first- and second-pulse interactions gated on time differences less than 0.7 μs. The bottom two panels show the time spectrum and second pulse interaction, gated on overload first interaction pulses.

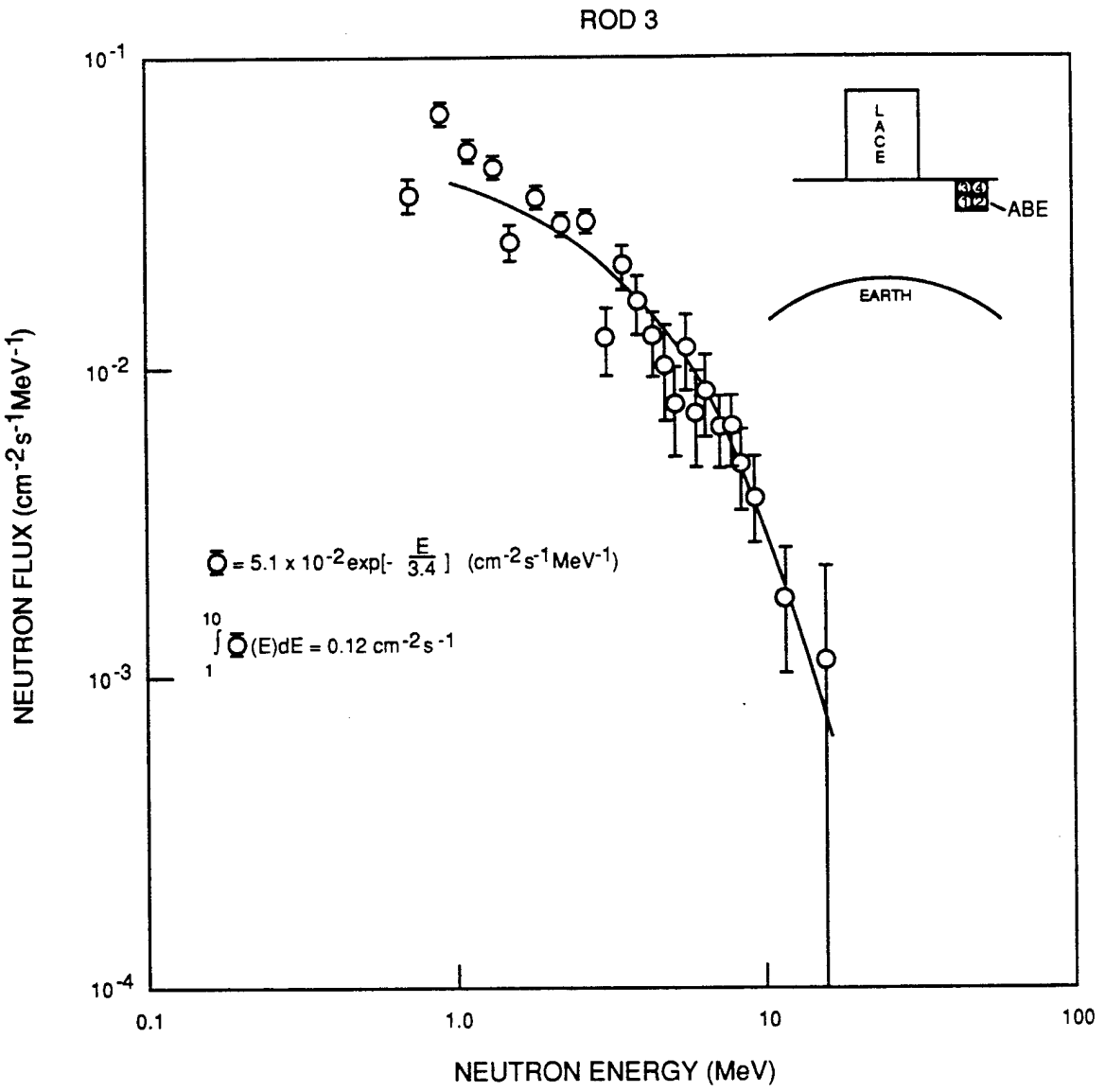

Figure 10. The neutron energy spectrum recorded by scintillator rod 3 during the first half of orbit 345 starting at 6:09 UT on 8 March 1990. As shown in the inset diagram at the upper right, rod 3 has a clear field of view of the LACE spacecraft and is shielded from the atmosphere leakage neutron flux by the other three rods.

and that here, as before, the distribution of second interaction pulse heights does not resemble that shown in Figure 8.

iv) Cosmic Ray-Generated Muons (U)

(U) A close inspection of the time spectrum given in the bottom left-hand panel of Figure 9, shows three separate components. Arguments have already been presented to support interpretation of the horizontal late-time component as due to chance coincidences, and the sharp, early-time upturn as due to afterpulsing. The intermediate ramp bears a close resemblance to a similar ramp shown in Figure 6. However, interactions causing these two similar time-difference components, yield markedly different second-interaction pulse-height spectra. Whereas neutron induced second interaction spectra cutoff above about 500 keV, the corresponding spectrum here extends beyond the upper equivalent electron energy range of the ABE ADCs. Other evidence to support an interpretation in terms of cosmic-ray-generated muons that result from interactions with the nuclear constituents of the LACE spacecraft are: 1) A linear-least-squares fit of an exponential function to the ramp portion of the time spectrum corrected for chance coincidence yields a time constant of 2.0 ± 0.15 μs. This value is close to the mean life of a muon at rest, $\tau = 2.15$ μs. 2) In the half of orbit 345 chosen for study here, events consistent with a muon interpretation occurred far more frequently (a factor of close to 20 to 1) in that scintillator rod (rod number 3) having a free field of view of the spacecraft than in the one (rod number 2) shielded by the other three from viewing the spacecraft directly. This signature is expected if the cause of the events is a spacecraft-generated muon because its mean time to beta decay is sufficiently short that most of those produced in the Earth's atmosphere should never reach the orbit of LACE (at 550 km altitude) before decay.

v) Preliminary Energy Spectrum of Neutrons (U)

(U) The foregoing analysis of backgrounds can be used to develop a filter for event-mode data that will maximize the true neutron signal to background ratio. Study of Figures 6 and 7 show that subtraction of the chance coincidence spectrum measured during a late time-difference interval spanning 17 μs to 25 μs, from the total spectrum measured during an early time-differences interval spanning 1.4 μs to 4.7μs, should be optimal. This choice will maximize the neutron signal but avoid most of the afterpulsing events. If, in addition, we require simultaneously that the second-interaction pulse height should be less than 0.15 MeV, then Figures 8 and 9 show that effects of afterpulsing can be further reduced. Although this last choice reduces the ABE efficiency by a factor of 1.7 because of the loss of detection of the 478 keV gamma ray, it reduces the addition of a contribution to the high-energy portion of the neutron spectrum due to afterpulsing.

(U) Because of space limitations we will only mention here, without showing calibration data, the steps required to construct a neutron flux spectrum from the pulse-height distribution measured using ABE. Details will be given in a later paper. Spectra are recorded in four overlapping, 64-channel intervals. The amplification gains within succeeding intervals differ by roughly a factor of 5.6 thereby providing a dynamic range in equivalent electron energy of about a factor of 10^3. Pre-launch pulser and gamma-ray calibrations are used to adjust the four different spectra to form a single spectrum spanning the energy range between about 40 keV and 20 MeV. Adjustments are made in this step to correct for both the differential and integral nonlinearities of each of the five ADCs in the instrument. The next step translates the equivalent electron energy scales of the four ADCs into neutron energy using Van de Graaff calibration data obtained at Los Alamos. A final step corrects the measured energy-dependent count rates by efficiency factors calculated using the Monte Carlo Neutron-Photon transport code, MCNP. The relative energy dependence of these efficiencies was checked by comparing the spectrum of ^{252}Cf fission neutrons measured at NRL with the best known spectrum tabulated by Madland *et al.* (1986). The comparison was excellent. The absolute magnitude of the efficiency was checked by measuring the spectrum of a known intensity $^{241}Am-^{11}B$ neutron source at Los Alamos. Inferred and known intensities agreed

to within 10%. A multiplicative factor due to dead-time effects, inferred from the time distribution of second interactions relative to detection of a first interaction, is applied to the final neutron spectrum.

(U) The resultant spectrum from rod number 3 accumulated over the half of orbit 345 starting at 6:09 UT on 8 March, 1990, is shown in Figure 10. Rod three was chosen because, in the short time interval of ABE data studied here, it accumulated the most counts. Although, as seen in the inset diagram in the upper right of the figure, this rod views the spacecraft directly and is mostly shielded from atmospheric neutrons, its measured flux spectrum is, to zeroth order, representative of that seen by the other three rods. Integration between 1 and 10 MeV yields $\Phi(1-10) = 0.12$ cm^{-2} s^{-1}. This value compares favorably with the average intensity measured by Jenkins *et al.* (1970) aboard the OGO 6 spacecraft using a moderated ^{3}He tube, $\Phi(1-10) = \sim 0.15$ cm^{-2}s^{-1}. This agreement lends confidence to our ultimate ability to meet all requirements of the space neutron background needed for development of a mass sensor for the NPB program. The advancement of ABE over the OGO 6 experiment is that it will be able to provide the first detailed neutron energy spectrum spanning 0.5 to 20 MeV. Although our analysis has not proceeded far enough yet, we also hope to infer, for the first time, the neutron spectrum generated by interactions between galactic cosmic rays and the nuclear constituents of a spacecraft. A check on the intensity of this spectrum will be provided by the detected muon intensity, resulting from the decay of pions generated in the spacecraft.

ACKNOWLEDGMENTS (U)

(U) Many people contributed to the success of the Army Background Experiment. It was a collaboration between Grumman Corporation and Los Alamos supported by the U.S. Army Strategic Defense Command. Special credit for this success goes to the dedicated team at Los Alamos responsible for the design, fabrication, and testing of the instrument. Leading individuals in this effort were 1) Don Enemark who led the technical effort, 2) Darrell Call who designed the GSE operating systems, 3) Jerry Longmire who designed the analog electronics, 4) Frank McGirt who was responsible for the GSE hardware design, 5) Gregg Obbink who was responsible for mechanical fabrication, 6) Mick Piotrowski who was responsible for the mechanical design, 7) Tony Rose who designed the GSE interface, 8) Ken Spencer who was responsible for electronic testing, 9) Max Seamons who designed and implemented the microprocessor software, and 10) Glenn Thornton who helped in the digital design of the electronics. Bob Scarlett provided program management. This prelaunch effort was augmented by Dick Anderson and Marilyn Halbig who developed the post-launch data reduction codes for ABE. Special thanks are also given to the whole crew at NRL and its subcontractors that bent over backwards to accommodate ABE into an already-designed spacecraft and made the experience both fun and rewarding. Finally, this work was done under the auspices of the U.S. Department of Energy.

REFERENCES (U)

Jenkins, R. W., J. A. Lockwood, S. O. Ifedilli, and E. L. Chupp, *J. Geophys. Res.*, **75**, 4197, 1970.

Madland, D. G., R. J. Labauve, and J. R. Nix, Nuclear Standard Reference Data IAEA-TECDOC-335 (IAEA, Vienna, Austria, 1985.